Geometry and Framework Interactions of Zeolite-Encapsulated Copper(II)−Histidine Complexes

Roeland Grommen,[†] Palanichamy Manikandan,[‡] Yong Gao,[‡] Tania Shane,[‡] Johan J. Shane,[‡] Robert A. Schoonheydt,[†] Bert M. Weckhuysen,*[,†] and Daniella Goldfarb*[,‡]

Contribution from the Department of Chemical Physics, The Weizmann Institute of Science, Rehovot-76100, Israel, and Centrum voor Oppervlaktechemie en Katalyse, Departement Interfasechemie, K.U.Leuven, Kardinaal Mercierlaan 92, 3001 Leuven, Belgium

Received July 13, 2000. Revised Manuscript Received September 8, 2000

Abstract: The coordination geometry of zeolite-encapsulated copper(II)−histidine (CuHis) complexes, prepared by ion exchange of the complexes from aqueous solutions into zeolite NaY, was determined by a combination of UV−vis−NIR diffuse reflectance spectroscopy (DRS), X-band EPR, electron-spin−echo envelope modulation (ESEEM), and high field (W-band) pulsed ENDOR techniques. X-band EPR spectroscopy detected two distinct complexes, **A** and **B**, which are different from the prevailing Cu(II) bis-His complex in the exchange solution (pH 7.3 with a His:Cu(II) ratio of 5:1). Moreover, the relative amount of complex **B** was found to increase with increasing Cu(II) concentration. The EPR parameters of complex **A** are $g_\perp = 2.054$, $g_\parallel = 2.31$, and $A_\parallel = 15.8$ mT, whereas those of complex **B** are $g_\perp = 2.068$, $g_\parallel = 2.25$, $A_\parallel = 18.3$ mT, and $A_\perp(^{14}\text{N}) \sim 1.3$ mT. The presence of the ^{14}N superhyperfine splitting shows that in complex **B** three nitrogens are coordinated to the Cu(II). Furthermore, DRS exhibits a shift of the d−d absorption band of Cu(II) from 15 200 cm^{-1} in complex **A** to 15 900 cm^{-1} in complex **B**, indicating an increasing ligand field strength in the latter. The coordination of the imino nitrogen of the imidazole group was detected in the two complexes via the ESEEM frequencies of the remote nitrogen. In contrast, only complex **A** exhibited ^{27}Al modulation, which indicates that the Cu(II) binds to zeolite framework oxygens. ^{2}H and ^{1}H W-band ENDOR measurements on samples where the exchangeable protons were replaced with ^{2}H, and using specifically labeled histidine (His-α-*d*-*β*-d_2), lead to the unambiguous determination of the coordination configuration of the two complexes. Complex **A** is a mono-His complex where both the amino and imino nitrogens are coordinated and the other equatorial ligands are provided by a zeolite oxygen and a water molecule. Complex **B** is a bis-His complex, which is situated in the center of the supercage, and all equatorial coordination sites are provided by the His molecules. These are amino and imino nitrogens of one His molecule and the imino nitrogen and carboxylate oxygen of the second His molecule. Complex **A** can be converted into complex **B** by stirring the zeolite in a high pH solution, whereas complex **B** is converted into complex **A** by using a low pH solution, thus indicating that complex **A** is stabilized by the presence of intrazeolitic protons. On the basis of the structure of the complexes, the dependence of their relative amounts on the pH and Cu(II) concentration in the exchange solution, the His:Cu(II) ratio in the zeolite, the amount of exchanged Na(I) ions, and the steric constraints imposed by the zeolite framework, a model for the ion exchange processes and the intrazeolite reactions leading to the formation of the two complexes is presented.

Introduction

One of the approaches for the preparation of redox-active zeolite catalysts is the encapsulation of transition metal complexes in the zeolite channels where the general idea is to combine the solution like activity with the shape-selective control induced by the zeolite. In addition to the space constraints imposed by the zeolite, the net negative charge of the zeolite framework and the distribution of the positive charges of the cations can lead to specific interactions with the zeolite framework which in turn induce structural and functional modification as compared to solution activities.[1−3] It has been shown that zeolite Y encapsulated copper(II)−histidine (CuHis) complexes exhibit promising catalytic activity in the epoxidation of alkenes with peroxides at relatively low temperatures.[4,5] These occluded complexes were characterized by diffuse reflectance spectroscopy (DRS) in the UV−vis−NIR region and X- and Q-band electron paramagnetic resonance (EPR) spectroscopies.[5] Under certain conditions the encapsulated CuHis complex gave rise to a well-resolved seven-line EPR superhyperfine splitting, which was assigned to a Cu(II) bis-His complex with three nitrogens and one oxygen in its first equatorial coordination sphere. However, depending on the concentrations of Cu(II) and His, and the pH of the exchange medium, several types of

* To whom correspondence should be addressed.
[†] Centrum voor Oppervlaktechemie en Katalyse.
[‡] The Weizmann Institute of Science.

(1) De Vos, D. E.; Knops-Gerrits P. P.; Parton, R. F.; Weckhuysen, B. M.; Jacobs, P. A.; Schoonheydt, R. A. *J. Inclus. Phenom. Mol. Recogn. Chem.* **1995**, *21*, 185−213.
(2) De Vos D. E.; Knops-Gerrits P. P.; Vanoppen D. L.; Jacobs P. A. *Supramol. Chem.* **1995**, *6*, 49−57.
(3) Kozlov, A.; Asakura, K.; Iwasawa, Y. *Microporous Mesoporous Maters.* **1999**, *21*, 571−579.
(4) Weckhuysen, B. M.; Verberckmoes, A. A.; Vannijvel, I. P.; Pelgrims, J. A.; Buskens, P. L.; Jacobs, P. A.; Schoonheydt, R. A. *Angew. Chem., Int. Ed. Engl.* **1995**, *34*, 2652−2654.
(5) Weckhuysen, B. M.; Verberckmoes, A. A.; Fu, L.; Schoonheydt, R. A. *J. Phys. Chem.* **1996**, *100*, 9456−9461.

10.1021/ja002572p CCC: $19.00
Published on Web 11/04/2000

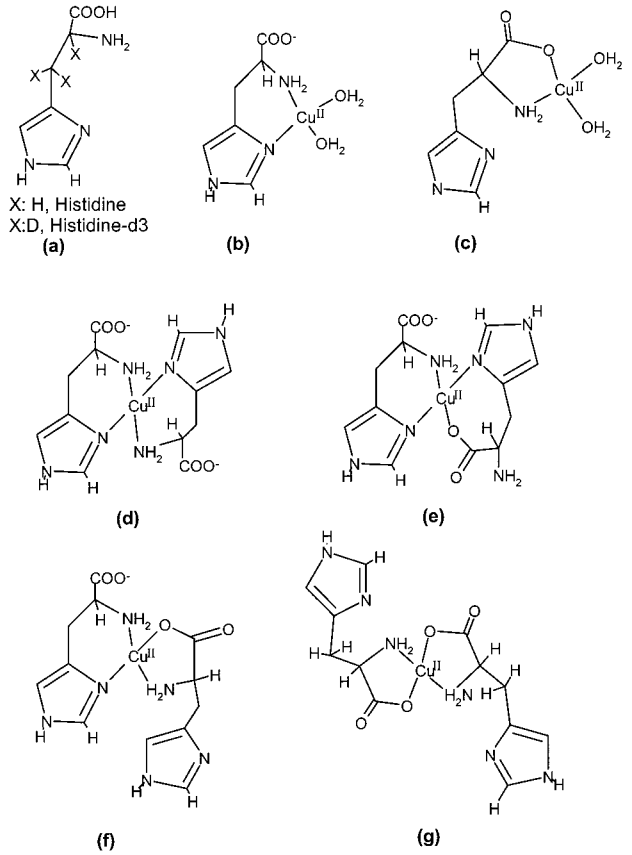

Figure 1. Molecular structures of the ligands used and possible models of His coordination in CuHis complexes: (a) His and His-α-d,β-d_2; (b and c) mono complexes with $N_{am}N_{im}O_wO_w$ and $N_{am}O_{COO}O_wO_w$ coordination, respectively; and (d−g) bis-complexes with $N_{am}(1)N_{im}(1)$-$N_{am}(2)N_{im}(2)$, $N_{am}(1)N_{im}(1)N_{im}(2)O_{COO}(2)$, $N_{am}(1)N_{im}(1)N_{am}(2)O_{COO}(2)$, and $N_{am}(1)O_{COO}(1)N_{am}(2)O_{COO}(2)$ coordination, respecively. The axial ligands are omitted in these representations.

complexes with different g and A values are formed. It is not clear what is the structural basis for these differences and what is the effect of the zeolite environment on the structure and chemical nature of the encapsulated complexes.

The coordination chemistry of CuHis in solution has been studied in great detail.[6−12] The His molecule contains three coordination sites, the amino nitrogen, N_{am}, the imidazole nitrogen, N_{im}, and the carboxylate oxygen, and therefore it can behave as a mono-, bi-, and tridentate ligand (Figure 1). Depending on the pH and the relative concentrations of Cu(II) and His, different complexes can be formed. This is illustrated in Table 1 for an aqueous solution of 1×10^{-3} M Cu(II) and 5×10^{-3} M His, as calculated with the chemical speciation program GEOCHEM.[13] At pH 2 only 0.83% of the Cu(II) is coordinated to His. At pH 3, Cu(II) forms primarily mono-His complexes, whereas in the pH range of 6−10 bis-His complexes, $Cu(His)_2$, are exclusively present.[6] Several studies report that an equilibrium between two different coordination configurations exists in solutions of $Cu(His)_2$ complexes.[9,12] In the first configuration the equatorial ligands are four nitrogens, N_{am} and N_{im} of each molecule ($N_{am}(1)N_{im}(1)N_{am}(2)N_{im}(2)$), as shown in Figure 1d, and the carboxylate oxygen may be coordinated in an apical position, though it is rather strained. In the above notation the number in parentheses refers to a specific His molecule. In the second configuration the carboxylate oxygen of one His ligand replaces one of the nitrogens, resulting in an $N_{am}(1)N_{im}(1)N_{am/im}(2)O_{COO}(2)$ binding mode in the equatorial plane (see Figure 1e,f). Using high field electron−nuclear double resonance (ENDOR) spectroscopy, we have recently shown that the frozen aqueous solution (pH 7.3) of $Cu(His)_2$ consists of a single complex (>90%) with the $N_{am}(1)N_{im}(1)N_{am}(2)N_{im}(2)$ configuration.[14]

Table 1. Concentrations of Mono-CuHis and Bis-CuHis Complexes in Aqueous Solutions with Different pH, as Obtained from Calculations Performed by PC-GEOCHEM with the Following Input Parameters: $[Cu(II)] = 10^{-3}$ M and $[His] = 5 \times 10^{-3}$ M and an Ionic Strength of 1 mM)

pH	% Cu(II) complexed	$[Cu(His)^+]$, M	$[Cu(His)_2^+]$, M
2	0.83	8.3×10^{-6}	1.76×10^{-10}
3	56.63	3.49×10^{-4}	2.17×10^{-4}
4	99.4	4.44×10^{-5}	9.50×10^{-4}
5	100	7.67×10^{-7}	9.99×10^{-4}
6	100	3.77×10^{-7}	1×10^{-3}
7	100	1.84×10^{-8}	1×10^{-3}
7.3	100	3.66×10^{-9}	1×10^{-3}
8	100	$5.44 \times 10^{--10}$	1×10^{-3}

The objectives of the present work were (i) to determine the structure of the various zeolite-encapsulated CuHis complexes and to compare the coordination of these CuHis complexes with the one prevailing in solution and (ii) to determine the intrazeolite chemistry that affects the structure of CuHis complexes and the experimental parameters that control their formation. A combination of X-band electron-spin−echo envelope modulation (ESEEM) and high field (W-band, 95 GHz) pulsed ENDOR techniques were applied to obtain a detailed picture of the Cu(II) coordination environment. One- and two-dimensional (2D) ESEEM experiments are most suitable for the detection of weakly coupled nuclei,[15] such as the remote ^{14}N in the coordinated imidazole group of His[16] and the ^{27}Al of the zeolite framework.[17] W-band pulsed ENDOR is most convenient for investigating weakly and strongly coupled protons and deuterons.[14] In the case of CuHis complexes high-field ^1H ENDOR measurements are superior to X-band ENDOR where signals of weakly coupled ^1H and strongly coupled ^{14}N overlap.[18] It will be shown that two distinct CuHis complexes, differing in their first coordination shell and their interaction with the zeolite framework, are present in the supercages of zeolite Y. On the basis of the structural properties of these complexes, along with the effect of pH on their relative amounts

(6) Martell, A. E.; Smith, R. M. *Critical Stability Constants, Amino Acids*; Plenum Press: New York, 1974; Vol. 1.
(7) Sakurai, T.; Yamauchi, O.; Nakahara, A. *Bull. Chem. Soc. Jpn*. **1978**, *51*, 3203−3208.
(8) Sigel, H.; McCormick, D. B. *J. Am. Chem. Soc*. **1971**, *93*, 2041−2044.
(9) Welmann, K. M.; Wong, B. K. *Proc. Natl. Acad. Sci.* **1969**, *64*, 824−827.
(10) Sarkar, B.; Wigfield, Y. *J. Biol. Chem.* **1967**, *242*, 5572−5577.
(11) Crawford, T. H.; Dalton, J. O. *Arch. Biochem. Biophys.* **1969**, *131*, 123−138.
(12) Sigel, H.; Griesser, R.; McCormick, D. B. *Arch. Biochem. Biophys.* **1969**, *134*, 217−227.
(13) GEOCHEM-PC version 2.0 is a descendant of the multipurpose chemical speciation program GEOCHEM, which is widely used by soil and environmental chemists.
(14) Manikandan, P.; Epel, B.; Goldfarb D. Submitted for publication.
(15) (a) Dikanov, S. A.; Tsvetkov, Y. D. *Electron Spin−Echo Envelope Modulation Spectroscopy*; CRC Press: Boca Raton, FL, 1992; pp 359. (b) Schweiger A. In *Modern Pulse and Continuous-Wave Electron Spin Resonance*; Kevan, L., Bowman, M. K., Eds.; Wiley: New York, 1990; p 43.
(16) Jiang, F.; McCracken, J.; Peisach, J. *J. Am. Chem. Soc*. **1990**, *112*, 9035−9044.
(17) Matar, K.; Goldfarb, D. *J. Phys. Chem*. **1992**, *96*, 3100−3109.
(18) Werst, M. M.; Davoust, C. E.; Hoffman, B. M. *J. Am. Chem. Soc*. **1991**, *113*, 1533−1538.

Table 2. Chemical Analysis of Cu(His)-exchanged Y Samples

				chemical analysis			
sample	zeolite source	Si/Al	Cu(II)/UC[a]	Cu(II)/UC	N/UC	His/UC	His/Cu(II)
CuHisY-1v	Ventron	2.49	0.25	0.35	4.76	1.56	4.5
CuHisY-2v	Ventron	2.49	0.50	0.52	9.36	3.12	6.0
CuHisY-3v	Ventron	2.49	1.0	0.81	23.98	8.0	9.8
CuHisY-1t	TSZ	2.71	0.25	0.28	4.0	1.33	4.7
CuHisY-2ta	TSZ	2.71	0.50	0.45	5.53	1.84	4.1
CuHisY-3t	TSZ	2.71	1.0	0.37	5.10	1.70	4.5
CuHisY-4t	TSZ	2.71	1.5	1.05	10.47	3.49	3.3
CuHisY-1c5	Conateka	5.2	0.25	0.24	3.20	1.07	4.4
CuHisY-2c5	Conateka	5.2	0.50	0.43	5.53	1.84	4.3
CuHisY-3c5	Conateka	5.2	1.0	0.61	7.89	2.63	4.3
CuHisY-1c11	Conateka	10.9	0.25	0.22	2.78	0.93	4.2
CuHisY-2c11	Conateka	10.9	0.50	0.39	4.60	1.53	4.0
CuHisY-3x11	Conateka	10.9	1.0	0.60	6.49	2.16	3.6
CuHisY-1c24	Conateka	24	0.25	0.20			
CuHisY-2c24	Conateka	24	0.50	0.43	4.97	1.66	3.9
CuHisY-3c24	Conateka	24	1.0	0.55	4.77	1.59	2.9

[a] Determined from the Cu(II) concentration in the exchange solution and assuming complete exchange.

and chemical analysis of the ion exchange process, mechanisms for their ion exchange and intrazeolite transformations are proposed.

Experimental Section

Sample Preparation. Aqueous solutions of preformed CuHis complexes, prepared in doubly distilled water with a His:Cu(II) ratio of 5:1 at pH 7.3, were used for ion exchange with NaY (Ventron, Si:Al = 2.49; TSZ, Si:Al = 2.71; Conteka, Si:Al = 5.2, 10.9, 24). Experimental details on the sample preparation are given in previous publications.[4,5] Three types of zeolite samples, differing in their amounts of CuHis complexes, were prepared using solutions with different CuHis concentrations (1, 2, and 4 mM Cu(II) corresponding to 0.25, 0.5, and 1.0 Cu(II) per unit cell (UC), respectively) while keeping the His:Cu(II) ratio in the solution at 5:1 and the pH at 7.3. The pH was adjusted with 0.1 M NaOH and/or 0.1 M H_2SO_4. The zeolite samples are denoted as CuHisY-1x (0.25 Cu/UC), CuHisY-2x (0.5 Cu/UC), and CuHisY-3x (1.0 Cu/UC) where x = v, t, or c to denote the source of the zeolite (with v = Ventron, t = TSZ, and c = Conteka). Samples with 0.25 Cu/UC and 0.5 Cu/UC were also prepared with DL-histidine-α-d,β-d_2 (CDN isotopes, His-d_3, see Figure 1a) and hereafter referred to as CuHis-d_3Y-1t and CuHis-d_3Y-2t. In addition, samples of CuHisY-1t and CuHisY-2t were soaked in D_2O for 24 h at room temperature (RT), to replace exchangeable protons with deuterons. One sample with 0.5Cu(II)/UC, in a TSZ zeolite, was prepared from an exchange solution at pH = 4.0.

Samples of CuHisY-1t and CuHisY-3c24 were stirred for 24 h at RT in solutions of pH 4.0 (prepared with HCl) and 10.5 (prepared with NaOH), respectively. The pH was measured regularly and adjusted if needed. All samples were dried at 333 K after filtration. The samples prepared and their notations and compositions are summarized in Table 2. For reference purposes, aqueous solutions of CuHis solutions were also prepared with His:Cu(II) ratios of 5, 4, 3, 2, and 1 at pH 7.3, and with a His:Cu(II) ratio of 5 at pH 6 and 8.

Spectroscopy. DR spectra of the CuHis complex encapsulated zeolite samples were taken on a Varian Cary 5 UV−vis−NIR spectrophotometer at room temperature. The spectra were recorded against a halon white reflectance standard in the range 2500−200 nm. UV−vis measurements of the ion exchange solutions were done with a Perkin-Elmer Lambda 12 spectrophotometer.

Atomic absorption spectrometry (AAS) measurements were performed using an Instrumentation Laboratory Inc. apparatus with a nitrous oxide−acetylene flame. The light source was a hollow cathode lamp with a wavelength of 324.7 and 589.6 nm for the determination of Cu(II) and Na(I) ions, respectively. The His content was determined by the Micro-Kjeldahl method. The amounts of Cu(II) and His in the solid materials were determined after dissolution of known quantities of zeolite material in HF/H_2SO_4.

CW-EPR measurements were performed on a Varian-E12 spectrometer (~9 GHz) at ~150 K. ESEEM and hyperfine sublevel correlation (HYSCORE) experiments were carried out at 8.5 GHz and 4.2K using a home-built spectrometer.[19,20] The ESEEM measurements were obtained using the three-pulse sequence $\pi/2-\tau-\pi/2-T-\pi/2-\tau-$echo, with the appropriate phase cycle[21] and microwave (MW) pulse length, t_{MW}, of 0.02 μs. The HYSCORE measurements were carried out with the sequence $\pi/2-\tau-\pi/2-t_1-\pi-t_2-\pi/2-\tau-$echo, and a four-step phase cycle.[22,23] The pulse length of the $\pi/2$ and π pulses in these experiments was 0.02 and 0.04 μs, respectively. Four-pulse ESEEM experiments were carried out using the HYSCORE sequence with $t_1 = t_2$. The pulse length chosen is short enough such that its bandwidth affords simultaneous excitation of allowed and forbidden EPR transitions necessary for the observation of nuclear modulation from the nuclei of interest. Shorter pulses would require the full power of the spectrometer and lead to a longer dead-time. The HYSCORE experiments were recorded with a series of τ values to ensure that all frequencies are detected. In general short τ values were used to avoid significant echo decay due to the rather short phase memory time.

Prior to Fourier transformation (FT) of the ESEEM data the background decay was removed by a polynomial fit. The resulting time domain traces were convoluted with either an exponential or a Hamming window, zero filling was performed, and after FT the magnitude mode was selected. In the HYSCORE data the background decay in both t_1 and t_2 dimensions was removed using a third-order polynomial fit, the data were convoluted with a Hamming or sinbell function, and after zero filling to 512 points in each dimension FT was carried out in the two dimensions and magnitude spectra were calculated. The spectra shown are contour plots with a linear scaling of the contour intervals.

W-band (94.9 GHz) field sweep echo-detected (FS-ED) EPR and ENDOR measurements were carried out at 4.5 K on a home-built spectrometer described elsewhere.[24] FS-ED EPR spectra were recorded using the two-pulse echo sequence ($\pi/2-\tau-\pi-\tau-$echo) where the echo intensity is registered as a function of the magnetic field. The magnetic field value was determined from the ^{1}H Larmor frequency obtained from the ENDOR experiments. Typically, MW pulse lengths of 0.05 and 0.1 μs were employed with $\tau = 0.3$ μs. In principle shorter pulses can be used to obtain higher S/N. In our particular case the length of pulses was limited by the available power as only one MW channel was used. The ^{1}H ENDOR spectra were recorded using the Davies ENDOR sequence, $\pi-T-\pi/2-\tau-\pi-\tau-$echo, where an RF π pulse is introduced during the time interval T.[25] ^{2}H ENDOR spectra were recorded using the Mims ENDOR sequence, where the three-pulse sequence is used and a radio frequency (RF) π pulse is applied during the interval T.[26] The experimental conditions for the ^{1}H Davies ENDOR spectra were $t_{MW} = 0.2, 0.1, 0.2$ μs, $\tau = 0.5$ μs, $t_{RF} = 25$ μs. Relatively long MW pulses were employed because in the Davies ENDOR experiment selective pulses are needed for the observation of small hyperfine couplings. For ^{2}H Mims ENDOR, $t_{MW} = 0.1, 0.1, 0.1$ μs, $\tau = 0.25$ μs, $t_{RF} = 40$ μs. The MW pulse length was optimized for the strongest ENDOR effect and better results were obtained with longer pulses. In Davies and Mims experiments the length of the RF pulse was determined by the maximum available RF power in the cavity, and the shortest time delay at which a full clear echo can be observed was chosen for τ. The intensity and frequency scales of the ^{2}H spectra were multiplied by −1 and $\gamma^H/\gamma^D = 6.5144$, respectively, to allow a convenient comparison with the ^{1}H ENDOR spectra. The frequency

(19) Goldfarb, D.; Fauth, J. M.; Tor, Y.; Shanzer, A. *J. Am. Chem. Soc.* **1991**, *113*, 1941−1948.
(20) Shane, J. J.; Gromov I.; Vega, S.; Goldfarb, D. *Rev. Sci. Instrum.* **1998**, *69*, 3357−3364.
(21) Fauth, J. M.; Schweiger, A.; Braunschweiler, L.; Forrer J.; Ernst, R. R. *J. Magn. Reson.* **1986**, *66*, 74−85.
(22) Höfer P.; Grupp, A.; Nebenführ H.; Mehring M. *Chem. Phys. Lett.* **1986**, *132*, 279−282.
(23) Gemperle G.; Aebli G.; Schweiger A.; Ernst R. R. *J. Magn. Reson.* **1990**, *88*, 241−256.
(24) Gromov, I.; Krymov, V.; Manikandan, P.; Arieli, D.; Goldfarb, D. *J. Magn. Reson.* **1999**, *139*, 8−17.
(25) Davies, E. R. *Phys. Lett. A* **1974**, *47*, 1−2.
(26) Mims, W. B. *Proc. R. Soc.* **1965**, *283*, 452−457.

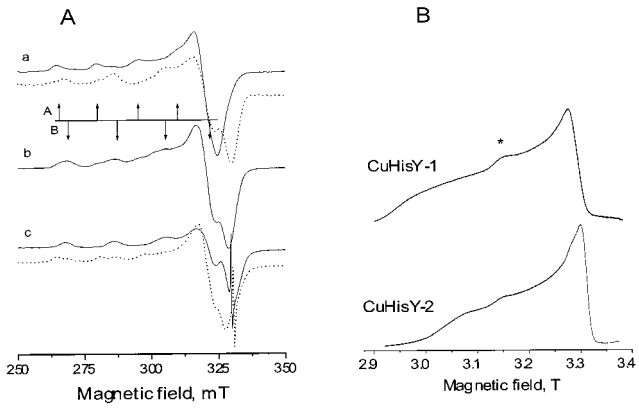

Figure 2. (A) CW X-band EPR spectra, recorded at 150 K, of (a) CuHisY-1t before (solid line) and after (dotted line) stirring in a pH 10.5 solution [the upward and downward arrows represent the $A_{||}$ features of complexes **A** and **B**, respectively]; (b) CuHisY-1t; and (c) CuHisY-3c24 before (solid line) and after (dotted line) stirring in a pH 4 solution. (B) FS-ED W-band EPR spectra (4.5 K) of CuHisY-1t and CuHisY-2t. The asterisk marks a signal of an unknown impurity.

scale in the ^{1}H and ^{2}H ENDOR spectra is given with respect to the Larmor frequency, $\nu = \nu_{RF} - \nu_H$.

Results

Chemical Analysis. All CuHis encapsulated zeolite samples were light blue and their Cu and nitrogen contents, which provides a measure of the His amount in the zeolite, are summarized in Table 2. The His:Cu(II) ratio in the zeolite is larger than 2, indicating that an excess of free His has been co-exchanged as His^+ into the zeolite. Moreover, this ratio is different from the ratio in the exchange solution where His:Cu(II) = 5, and it was found to depend on the Si:Al ratio and the Cu(II) content (see Table 2). It is clear that the His:Cu(II) ratio decreases with increasing Si:Al ratio showing that as the cation content of the zeolite decreases less His^+ is exchanged. The co-exchange of His^+ is confirmed by measurements of the amount of released Na(I) ions compared with the amount of Cu(II) taken up by the zeolite after ion exchange. A Na(I):Cu(II) ratio of 6−7 was obtained for the Ventron zeolites.

DRS and CW EPR Measurements. The X-band CW-EPR spectra of CuHisY-1t, CuHisY-2t, and CuHisY-3c24, recorded at 150 K, are shown in Figure 2A. The spectrum of CuHisY-1t (trace a in Figure 2A) consists of two distinct EPR subspectra: one corresponding to complex **A** with $g_{||} = 2.31$ and $A_{||} = 15.8$ mT, and the other to complex **B**, with $g_{||} = 2.25$ and $A_{||} = 18.3$ mT. The relative ratio of A and B in this particular sample is about 70:30. The spectrum of CuHisY-2t (trace b in Figure 2A) shows the presence of the same two complexes with a relative increase in the amount of **B** (ratio of ∼40:60). Although the relative amounts of **A** and **B** varied from preparation to preparation for samples with 0.25 Cu(II)/UC complex **A** was always the major species and could reach 80%. Similarly for samples with 0.5Cu(II)/UC, complex **B** is always dominant. Samples with 1.0 Cu(II)/UC consist almost always exclusively complex **B**, as shown in the spectrum of CuHisY-3c24 (trace c in Figure 2A). These two complexes appeared in all NaY zeolites investigated, independent of their source. A seven-line superhyperfine splitting on the $M_I(Cu) = -3/2$ feature, corresponding to $A_\perp(^{14}N)$ of about 1.3 mT, can often be observed in spectra of CuHisY-2 samples. This is due to the presence of three ^{14}N nuclei with rather similar hyperfine couplings in the first coordination sphere of the Cu(II) ion. In contrast, the spectra of CuHisY-1 do not show clear ^{14}N superhyperfine splitting.

Table 3. EPR Parameters and d−d Absorption Maxima of Zeolite Encapsulated Cu(His)-Complexes, Aqueous Cu(His) Solutions, and Some Reference Compounds

sample	$g_\perp$, $g_{||}$	$A_{||}$ (mT)	$A_\perp(^{14}N)$ (mT)	d−d abs band (cm^{-1})
CuHisY-1t: signal A	2.054, 2.31	15.8		15200
CuHisY-1t: signal B	2.068, 2.25	18.3		
CuHisY-2t: signal B	2.068, 2.25	18.3	1.3	15600
CuHisY-2t: signal A	2.054, 2.31	15.8		
Cu(His) solution at pH 7.3 with His:Cu(II) = 3, 4, 5[14]	2.058, 2.24	17.9		15600
Cu(His) solution at pH 6.0 with His:Cu(II) = 5	2.058, 2.24	18.0		15800
Cu(His) solution at pH 8.0 with His:Cu(II) = 5	2.058, 2.24	17.9		15600
galactose oxidase (NNNO)[27]	2.05, 2.24	17.9	1.51	15900
$Cu(NH_3)_4$ (NNNN)[28]	2.047, 2.24	18.4	1.33	
$Cu(imidazole)_4$ (NNNN)[28]	2.047, 2.26	17.8	1.48	
$Cu(glycine)_2$ (NNOO)[28]	2.052, 2.27	14.7	12.0	

The EPR spectra of the D_2O exchanged CuHisY-1t and CuHisY-2t samples were also measured and they are similar to those of the original samples with some minor variations in the relative intensities of the two complexes. CuHis-d_3Y-1t and CuHis-d_3Y-2t were prepared for the assignment of the proton's ENDOR signals and their spectra are similar to those of CuHisY-1t and CuHisY-2t samples and so are their D_2O exchanged samples. Reducing the pH of the solution to 4.0 and keeping the Cu(II) concentration at 0.5Cu(II)/UC led to a sample with mostly complex **A**, in contrast to a dominating complex **B** in the samples exchanged at pH 7.3. Table 3 lists the g and A values of complexes **A** and **B** in the samples investigated and of other related systems.

The DRS spectrum of CuHisY-1v exhibits Cu(II) d−d absorption bands with a maximum at 15 200 cm^{-1}, whereas for CuHisY-2v it is shifted to 15 600 cm^{-1} (see Table 3). This shows that the ligand field strength of the Cu(II) in complex **B** is higher than that in complex **A**, indicating an increase in the number of nitrogens in the first coordination sphere. This is in agreement with the trend observed in the EPR parameters of complexes **A** and **B** where the larger $g_{||}$ and the smaller $A_{||}$ of complex **A** indicate fewer nitrogens in the first coordination shell.[28,29]

It is possible to change the relative amounts of the **A** and **B** complexes in the zeolite by stirring the samples (24 h at RT) in a solution with the appropriate pH (the solution does not contain any Cu(II) or His). For example, stirring a sample of CuHisY-3c24, which consists of complex **B** only, in a pH 4.0 solution leads to a significant decrease in the relative intensity of **B** and the appearance of complex **A** (see the dotted trace in Figure 2A,c). In addition, a signal typical of free Cu(II) with $g_{||} = 2.38$ and $A_{||} = 12.2$ mT becomes aparent.[30] In contrast, stirring a CuHisY-1t sample containing mostly complex **A** in a 10.5 pH solution resulted in the reduction of the relative amount of complex **A** and a significant increase in the intensity of **B** (see the dotted trace in Figure 2A,a). We have also tried to ion exchange zeolites X and A with aqueous solutions of CuHis

(27) Lontie, R. *Copper Proteins and Copper Enzymes*; CRC Press: Boca Raton, FL, 1984; Vols. 1−3.
(28) Scholl, H. J.; Hüttermann, J. *J. Phys. Chem.* **1992**, *96*, 9684−9691.
(29) Peisach J.; Blumberg W. E. *Arch. Biochem. Biophys*. **1974**, *165*, 691−708.
(30) (a) Naccache, C.; Ben Taarit, Y. *Chem. Phys. Lett.* **1971**, *22*, 171−181. (b) Turkevich, J.; Ono, Y.; Soria, J. *J. Catal.* **1972**, *25*, 44−54.

complexes at pH 7.3, but no appreciable amounts of ion exchanged CuHis complexes could be detected in these zeolites.

ED-FS W-band EPR spectra of CuHisY-1t and CuHisY-2t exhibit a powder pattern characteristic of an axial *g*-tensor where the hyperfine splittings of ^{63,65}Cu and ^{14}N are not-resolved as a result of extensive broadening due *g*-strain at high fields (Figure 2B). These spectra provide a more accurate determination of the *g*-values, especially $g_\perp$, as listed in Table 3. The spectra of many samples, though not all of them, show a signal at $g = 2.15$, marked by an asterisk in Figure 2B. The relative intensity of this signal is very small and we do not know its origin. It may correspond to the $g_{||}$ feature of a negatively charged Cu(II) complex with an NNNN configuration.[29] It is, however, difficult to rationalize the presence of a negative complex. Due to its minute amounts we shall not discuss this "impurity" signal any further.

To summarize, the CW-EPR results show that two types of CuHis complexes are present in the zeolite supercage, complex **A** and complex **B**. Complex **B** has three nitrogens in its first coordination shell whereas in complex **A** the Cu(II) is coordinated to one or two nitrogens only. The relative amount of **A** and **B** depends on the concentration of the Cu(II) in the exchange solution and its pH. Once introduced into the zeolite, the two complexes can be interconverted by soaking the zeolites in a solution with the appropriate pH. Since the EPR and DRS results do not provide enough details regarding the structure of the complexes, ESEEM, HYSCORE, and ENDOR measurements were carried out as well.

ESEEM and HYSCORE Measurements. The three-pulse ESEEM time domain traces and ESEEM spectra of CuHisY-1t and CuHisY-2t, recorded at a magnetic field where the echo amplitude reaches a maximum (290.8 mT), are shown in Figure 3a. The time domain traces, recorded with $\tau = 0.2$ μs, show that CuHisY-2t exhibits significantly deeper modulations than CuHisY-1t. The ESEEM spectra were obtained from the sum of individual ESEEM waveforms recorded with τ in the range of 0.16−0.73 (steps of 0.03 μs) to eliminate the τ dependence of the modulation amplitudes.[31] Both spectra (Figure 3b) exhibit three lines, at 0.7, 1.4, and 4.0 MHz, which are typical for the remote ^{14}N of the imidazole ring.[16,32] At X-band, this nitrogen obeys the cancellation condition where in one of the electron spin manifolds the nuclear Zeeman interaction and the hyperfine interaction cancel each other, resulting in a zero effective field. Under these conditions the nuclear frequencies of this particular M_S manifold correspond to the nuclear quadrupolar resonance (NQR) frequencies ν_-, ν_0, and ν_+, which appear at 0.7 and of 1.4 MHz ($\nu_- \simeq \nu_0$).[16,32,33] The 4.0 MHz frequency corresponds to the nuclear double-quantum transition frequency, ν_{dq}, of the other M_S manifold. From these frequencies an isotropic hyperfine coupling constant, a_{iso}, of 1.5−2 MHz, a quadrupole coupling constant, e^2qQ/h, of 1.4 MHz, and an asymmetry parameter, $\eta \sim 0.9$, are obtained.[16,32] The small splitting of the 0.7 MHz line indicates that $\eta < 1$. The positions of these NQR lines do not change when the external magnetic field is varied along the EPR powder pattern.

While the ^{14}N peaks in the CuHisY-1t spectrum are considerably weaker than those in CuHisY-2t, it exhibits an additional peak at 2.8 MHz that coincides with the ^{27}Al Larmor frequency and is therefore assigned to the ^{27}Al nuclei in the zeolite framework. This assignment was verified by the field dependence of this signal as shown in the inset of Figure 3b. It was obtained by performing the ESEEM experiments at various magnetic fields within the EPR powder pattern. This dependence excludes the possibility that this line is a combination frequency, $2\nu_+$, arising from the presence of two coupled remote nitrogens,[34] that is expected to be almost field independent. Combination peaks, providing direct evidence for two-imidazole coordination,[34] were not detected in the spectra of CuHisY-2 samples. The NaY Ventron zeolites show the same ESEEM spectra as the TSZ zeolites described above.

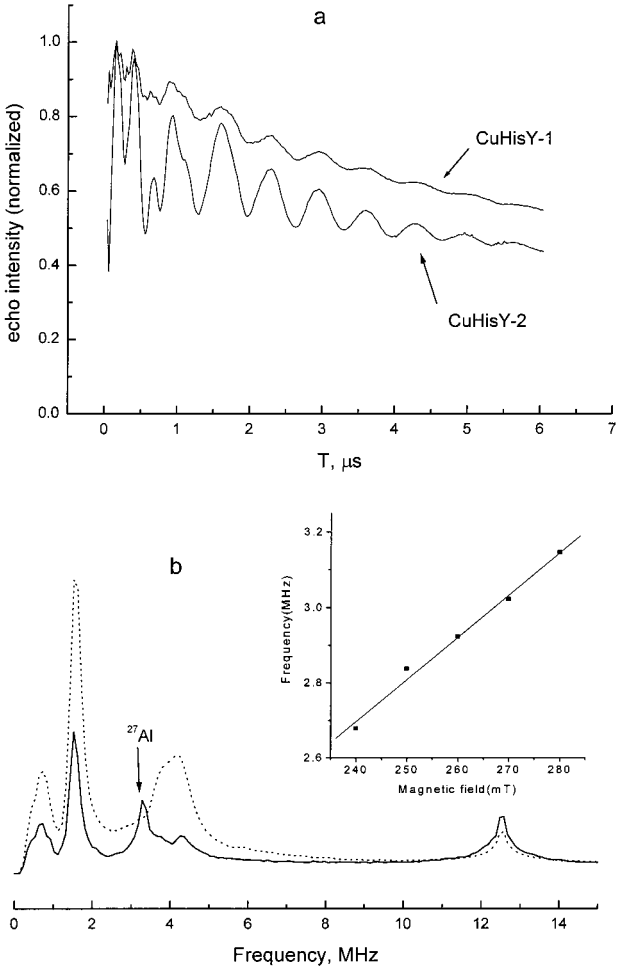

Figure 3. (a) Three-pulse ESEEM spectra of CuHisY-1t and CuHisY-2t recorded at 290 mT, $\tau = 0.2$ μs, and $T = 4.2$ K; (b) ESEEM spectra of the sum of the time domain ESEEM traces of CuHisY-1t (solid) and CuHisY-2t (dotted) recorded with τ in the range of 0.16−0.73 (steps of 0.03 μs). The insert shows the dependence of the frequency of the ^{27}Al peak on the magnetic field within the EPR powder pattern of the CuHisY-1v sample.

The above assignments were confirmed by the HYSCORE spectrum of CuHisY-1v, shown in Figure 4, which exhibits cross-peaks at ($\nu_-(\nu_0)$, ν_{dq}) and (ν_+, ν_{dq}) in both the (+, +) and (−, +) quadrants. The ^{27}Al peak appears on the diagonal and does not exhibit any correlations, as expected for a nucleus experiencing a very small hyperfine coupling. This, again, rules out the possible assignment of the 2.8 MHz peak to $2\nu_+$.

To summarize, the ESEEM experiments showed that complex **A** exhibits ^{27}Al modulations and the Cu(II) is coordinated to a smaller number of N_{im} than in complex **B**, which in turn does not interact with ^{27}Al. The proton region in the ESEEM spectra

(31) Mims, W. B. *Phys. Rev. B* **1972**, *6*, 3543−3545.
(32) Mims, W. B.; Peisach, J. *J. Chem. Phys.* **1978**, *69*, 4921−4930.
(33) Flanagan, H. L.; Singel, D. J. *J. Chem. Phys.* **1987**, *87*, 5606−5616.
(34) McCracken, J.; Pember, S.; Benkovic, S. J.; Villafranca, J. J.; Miller, R. J.; Peisach, J. *J. Am. Chem. Soc.* **1988**, *110*, 1069−1074.

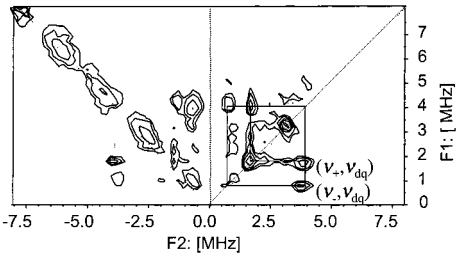

Figure 4. A 2D HYSCORE spectrum of CuHisY-1 recorded at $B_0 =$ 288 mT, $\tau = 0.24$ μs, and $T = 4.2$ K. The assignments of the cross-peaks are shown on the spectrum.

did not show any fine structure that could lead to the identification of the various protons. Four-pulse ESEEM experiments, used to determine proton shifted sum-combination peaks, were carried out as well to identify protons with different anisotropic hyperfine couplings.[35] The experiments were carried out at the $g_\perp$ position. In both CuHisY-1v and CuHisY-2v, a single rather broad shifted peak was detected, with a shift in the range of 1−1.66 MHz, depending on the τ value and the field at which the experiment was performed. This corresponds to an anisotropic hyperfine component in the range of 4.5−6 MHz. These results are not sufficient to differentiate the various types of coupled protons and we therefore turned to ENDOR spectroscopy.

ENDOR Measurements. While ESEEM measurements are most sensitive to the remote nitrogen in the coordinated imidazole group, the signals of the directly coordinated N_{im} and N_{am} nuclei and the coupled protons should appear in the ENDOR spectrum. X-band pulsed ENDOR spectra of the encapsulated complexes were measured at different magnetic fields along the EPR powder pattern (not shown for brevity). The spectra were poorly resolved and did not allow unambiguous assignments of the ^{14}N and ^{1}H signals. In contrast, high-quality ^{1}H spectra and ^{2}H spectra of exchangeable protons were readily obtained at W-band.

Our recent W-band ENDOR study of CuHis in solution[14] showed that four types of protons can be identified (see Figure 1) and their hyperfine couplings serve as signatures for the various coordination modes of His. The proton on the α-carbon, H_α, assumes a surprisingly large isotropic hyperfine coupling (10.9 MHz) when both N_{im} and N_{am} of the same histidine ligand are coordinated, forming a six-membered chelating ring which we refer to as a $N_{im}N_{am}$ ring. In contrast, the coupling of H_ϵ, the proton on the carbon next to the bound imino nitrogen, is significantly smaller ($A_{xx} = \pm 1.0$, $A_{yy} = \pm 2.40$, $A_{zz} = \mp 5.4$ MHz) and is not sensitive to whether N_{am} is coordinated or not. The amino protons ($H_{am1,2}$) exhibit rather large and anisotropic hyperfine interactions when N_{am} is coordinated ($A_{xx1} = \pm 6.0$, $A_{yy1} = \pm 7.0$, $A_{zz1} = \pm 14.0$ MHz, $A_{xx2} = \pm 6.0$, $A_{yy2} = \pm 10.0$, $A_{zz2} = \pm 14.0$ MHz), and as H_ϵ, the coupling is not affected significantly by the binding of the other nitrogen. The fourth type of protons are the protons on the β-carbons, H_β, that exhibit small hyperfine couplings ($A < 0.6$ MHz).[14]

Figure 5 summarizes the W-band pulsed ENDOR spectra of CuHisY-2t and CuHis-d_3Y-2t (both with ∼80% complex B) measured at the $g_\perp$ position. The ^{1}H ENDOR spectrum of CuHisY-2t, Figure 5a, consists of the signals of all coupled protons. It exhibits all the features observed in the corresponding spectrum of the exchange solution[14] with the exception of an additional powder pattern with singularities at ±2.56(0.1) and ±1.36(0.05) MHz, where the number in parentheses specifies

(35) Tyryshkin, A. M.; Dikanov S. A.; Goldfarb D. *J. Magn. Reson. A* **1993**, *105*, 271−283.

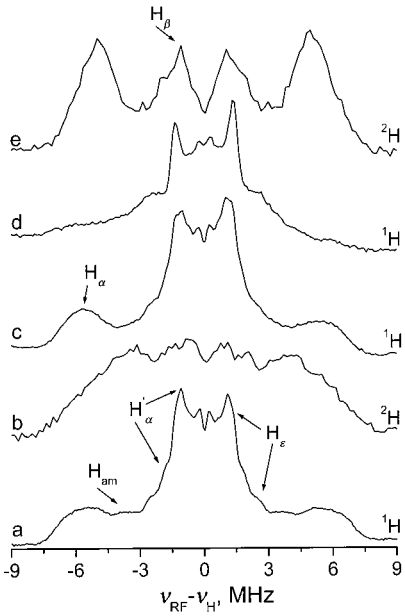

Figure 5. (a) ^{1}H Davies ENDOR spectrum of CuHisY-2t; (b) ^{2}H Mims ENDOR spectrum of CuHisY-2t exchanged in D_2O; (c) ^{1}H Davies ENDOR spectrum of CuHisY-2t exchanged in D_2O; (d) ^{1}H Davies ENDOR spectrum of CuHis-d_3Y-2t; and (e) ^{2}H Mims ENDOR spectrum of CuHis-d_3Y-2t. All spectra were recorded at 94.9 GHz, 4.5 K and at $g_\perp$. The frequency scales of the ^{2}H spectra were multiplied by γ_H/γ_D and the intensity scales by −1, to allow convenient comparison with the ^{1}H Davies ENDOR spectra.

the uncertainty. Accordingly, the signals at ±6.1(0.5) MHz are attributed to the H_α in a $N_{im}N_{am}$ ring. Similarly, the H_{am} signal can be identified from the ^{2}H and ^{1}H ENDOR spectra of CuHisY-2t exchanged with D_2O (Figure 5, b and c, respectively) where overlapping signals due to water coordination cannot be excluded. The assignment of the H_α signals is also confirmed by the ^{1}H and ^{2}H ENDOR spectra of the CuHis-d_3Y-2t (Figure 5d, e) sample. Apart from the signals of H_α and H_{am}, two superimposed powder patterns (±2.56(0.1), ±1.93(0.1), ±1.36-(0.05), and ±1.12(0.05) MHz) appear in the center of the spectrum (Figure 5a) and are due to nonexchangeable protons. One of these two powder patterns, ±1.93(0.1) and ±1.12(0.05) MHz, is absent from the ^{1}H ENDOR spectrum of CuHis-d_3Y-2t (Figure 5d) and is therefore associated with H_α or H_β. Since these couplings are too large for the H_β protons which are relatively far from the Cu(II) ion, they are attributed to H_α of a second His ligand, referred to as H'_α. The remaining signals, at ±2.56(0.1) and ±1.36(0.05) MHz, are due to the powder pattern of H_ϵ of an imidazole group. All these ENDOR spectra show that complex **B** has either an $N_{im}(1)N_{am}(1)N_{am}(2)O$ or an $N_{im}(1)N_{am}(1)N_{im}(2)O$ configuration.

The ENDOR spectra of CuHisY-1t and CuHis-d_3Y-1t (containing ∼70% complex **A**) are shown in Figure 6. The presence of H_α in a $N_{am}N_{im}$ chelating ring is evident from the ^{1}H and ^{2}H ENDOR spectra of CuHis-d_3Y-1t (Figure 6d,e). However, the doublet of H_α is not as resolved in Figure 6a as compared to that of the CuHisY-2t sample (Figure 5a). This is mainly due to overlap with signals of water protons in this region. In addition, only one powder pattern, corresponding to the imidazole proton (H_ϵ), is observed in the center of the spectrum at ±2.56(0.1) and ±1.36(0.05) MHz. This indicates that only one type of H_α, typical of $N_{am}N_{im}$ coordination, is present. This assignment is further supported by the ^{1}H and ^{2}H ENDOR spectra of CuHis-d_3Y-1t (Figure 6d,e), which is dominated by the powder pattern of H_ϵ. Note that the ^{1}H ENDOR spectra of

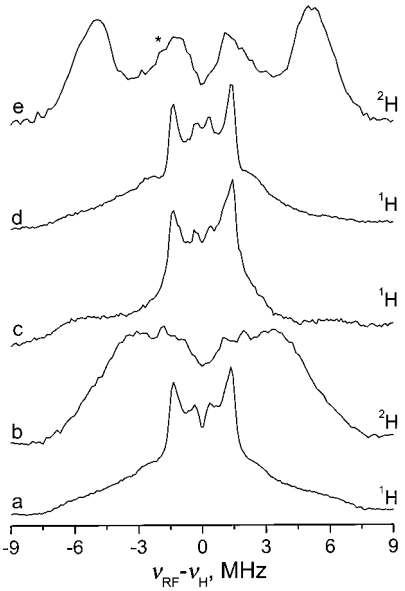

Figure 6. (a) ^{1}H Davies ENDOR spectrum of CuHisY-1t; (b) ^{2}H Mims ENDOR spectrum of CuHisY-1t exchanged in D_2O; (c) ^{1}H Davies ENDOR spectrum of CuHisY-1t exchanged in D_2O; (d) ^{1}H Davies ENDOR spectrum of CuHis-d_3Y-1t; (e) ^{2}H Mims ENDOR spectrum of CuHis-d_3Y-1t. All spectra were recorded at 94.9 GHz, 4.5 K and at $g_\perp$. The frequency scales of the ^{2}H spectra were multiplied by γ_H/γ_D and the intensity scales by -1, to allow convenient comparison with the ^{1}H Davies ENDOR spectra.

CuHis-d_3Y-2t and CuHis-d_3Y-1t are very similar. Hence, the most probable configuration of complex **A** is $N_{im}(1)N_{am}(1)OO$. The appearance of the signals marked by an asterisk in the ^{2}H spectrum of the CuHis-d_3Y-1t are due to H_α from a His ligand coordination only via one nitrogen and are attributed to a minor contribution of complex **B** present in the sample.

Discussion

The Structure of the Different Encapsulated CuHis Complexes. In the present investigation, the ion exchange process of incorporating preformed CuHis complexes into zeolite Y and the structure of the complexes encapsulated in the supercage have been studied as a function of the Cu(II) exchange level. The presence of bis-complexes in the pH 7.3 exchange solution has been implied by the application of the multipurpose chemical speciation program GEOCHEM[13] and earlier reports.[6−12] Our recent high-field ENDOR investigation of CuHis complexes in solution[14] showed that the primary configuration at this pH is $N_{am}(1)N_{im}(1)N_{am}(2)N_{im}(2)$.[14] The constrained zeolite environment with its high surface charge density and charge balance requirements induces changes in the overall stability of the CuHis complexes when they are incorporated into the zeolite, resulting in a change in coordination geometry. Therefore, in contrast to the exchange solution where only one type of complex is present in significant amounts, two different CuHis complexes, labeled as **A** and **B**, were identified within the zeolite cages, showing, in general, a preferential coordination of Cu(II) with the N atoms of the His ligand over the oxygens of the zeolites framework. In this section, we discuss the structure of complexes **A** and **B** as determined from the DRS, EPR, ESEEM, and ENDOR measurements, while in the next section we propose a mechanism for their formation and identify the factors stabilizing each one of them.

The two main differences between complexes **A** and **B**, detected by ESEEM, are the strong ^{27}Al peak and the weaker remote $^{14}N_{im}$ signals of complex **A**, as opposed to the absence of an ^{27}Al peak and intense remote $^{14}N_{im}$ signals in complex **B**. The ^{27}Al signal in the spectra of **A** indicates that this complex is situated close to the zeolite framework. Hence, on the basis of space consideration, this complex is located in the supercage and has only one His ligand where the other ligands are supplied by the zeolite and a water molecule. Moreover, The ENDOR results show that a chelating $N_{im}N_{am}$ ring is present and therefore we assign complex **A** to $N_{am}(1)N_{im}(1)O_ZO_W$, as shown in Figure 7a, where O(Z) symbolizes a zeolite oxygen.

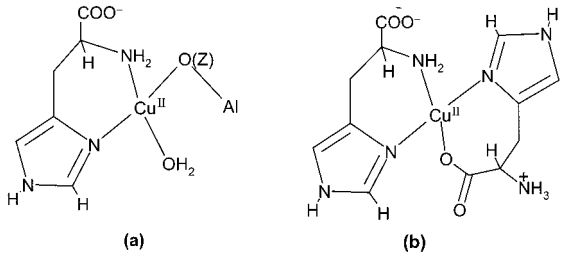

Figure 7. The structure of CuHis complexes in the zeolite Y: (a) complex **A** with $N_{am}(1)N_{im}(1)O_ZO_W$ coordination and (b) complex **B** with $N_{am}(1)N_{im}(1)N_{im}(2)O_{COO}(2)$ coordination.

The absence of the ^{27}Al signal in the ESEEM spectra of sample CuHisY-2 indicates that complex **B** is a bis-His complex situated in the center of the supercage, and the Cu(II) is not coordinated to the framework. This is in agreement with the ^{14}N superhyperfine splitting observed in the X-band EPR spectrum and the ENDOR results showing the presence of two types of H_α signals, one characteristic of a $N_{im}N_{am}$ ring and one of either N_{im} or N_{am} coordination. This assignment is also supported by the higher ligand field strength of complex **B** manifested by the higher frequency of the d−d absorption band, the smaller $g_{||}$ value, and the larger $A_{||}$.[29] The presence of a significantly stronger ^{14}N modulation of the remote nitrogen in the ESEEM spectrum of complex **B** compared to that of complex **A** leads to the conclusion that the coordination is $N_{im}(1)N_{am}(1)N_{im}(2)O_{COO}(2)$ (Figure 7b) and not $N_{im}(1)N_{am}(1)N_{am}(2)O_{COO}(2)$ as was previously suggested on the basis of DRS and CW EPR measurements only.[4,5] The positive charge of the complex then comes from the NH_3^+ group (with a pK_a value of 8.0) of the second His molecule.

Ion Exchange Process and Coordination Chemistry. Chemical analysis showed that for each CuHis complex exchanged into the zeolite, 6−7 Na(I) ions leave the zeolite. These results show that only preformed positively charged CuHis complexes are introduced into the zeolite and that His^+ is co-exchanged. Moreover, the difference between the His:Cu(II) and Na(I):Cu(II) ratios indicates that charge compensation by co-exchange of protons occurs as well, leading to some residual acidity in the zeolite. These acidic sites are responsible for the hydrolysis of cyclohexenoxide, which is formed during the oxidation of cyclohexene in the presence of *tert*-butyl hydroperoxide.[4,5] The amounts of co-exchanged His^+ and protons depend on the Si:Al ratio and the Cu(II) content in the exchange solution. The ability of charged CuHis complexes to exchange Na(I) ions depends on their charge and stability, which are both pH dependent. The stability and overall charge of CuHis complexes in solution are directly determined by the pK_a value of the imino nitrogens in the His ligand,[4,5] which is 6.5.[6] At a pH of 7.3, the pH of the exchange solution used in this work, all Cu(II) ions are coordinated to His molecules forming a bis-complex (Table 1) and the complexation constant, expressed as log K_c, of this complex is equal to 5.5.[6] Our earlier ENDOR study showed that the majority of the bis-complexes in solution have the $N_{im}(1)N_{am}(1)N_{im}(2)N_{am}(2)$ configuration and are

therefore expected to be neutral which prevents them from exchanging into the zeolite. The solution must therefore contain at least small amounts of some positively charged bis-complexes with the configurations of $N_{im}(1)N_{am}(1)N_{im}(2)O_{COO}(2)$ and/or $N_{im}(1)N_{am}(1)N_{am}(2)O_{COO}(2)$ and maybe very small amounts of positively charged mono-complex that are selectively exchanged into the zeolite. This selective exchange of positively charged complexes is one of the reasons for the differences in the structure of CuHis in solution and encapsulated in the zeolite. At pH 7.3 5.2% of the excess His molecules in the solution are positively charged and can also exchange zeolite Na(I) ions. Except for the charge of the species, the exchange is also influenced by the zeolite structure and/or composition which determine the space available. This explains why CuHis complexes cannot be exchanged into zeolite A where the cage is smaller and crowded with cations. Similarly, changes in the coordination geometry of the tetrapyridine copper(II) complex as compared to the solution structure were observed upon its introduction into NaY and MCM-41 due to space constraints and interaction with the host.[36,37]

An interesting observation of the present study is dependence of the relative amount of the encapsulated mono- (complex **A**) and bis-complexes (complex **B**) on the Cu(II) concentration of the exchange solution. At low Cu(II) concentrations, which leads to lower Cu(II) loading in the zeolite, the mono-complex prevails, whereas at higher Cu(II) concentrations, and thus higher Cu(II) loadings in the zeolite, the bis-complex is favored. Moreover, complex **B** can be converted into complex **A** in the zeolite cage by mixing the zeolite with a low pH solution according to

$$Cu(His)_2^+(Z) + H^+(S) + Na^+(Z) \leftrightarrow Cu(His)^+(Z) + His^+(Z) + Na^+(S) \quad (1)$$

where Z and S correspond to the zeolite and exchange solution, respectively. Similarly, complex **A** can be converted into complex **B** by mixing with a high-pH solution:

$$Cu(His)^+(Z) + His^+(Z) + OH^-(S) + Na^+(S) \leftrightarrow Cu(His)_2^+(Z) + H_2O(S) + Na^+(Z) \quad (2)$$

Processes 1 and 2 account for the interconversion between the two types of complexes, and suggest that at low Cu(II) loading, the mono-complex **A** prevails due to the higher proton concentration in the zeolite. Thus, the relative amount of protons in the zeolite determines if the nitrogen atom of the imidazole ring (with a pK_a value of 6.5) will be protonated or not. Protonation will lead to the formation of His^+, which will not coordinate to Cu(II), and thus the bis-His complex breaks up into a mono-His complex and a His^+ molecule, which is weakly coordinated to a $[Si-O-Al]^-$ cation exchange site. The reverse reaction takes place when deprotonation prevails. In this case, the His molecule will replace the zeolite oxygen according to the spectrochemical series because zeolite oxygens are harder ligands in comparison with nitrogen atoms. The overall result is the formation of a bis-His complex.

The stabilization of complex **A** can be explained by two possible models. In the first model a positively charged bis-complex is exchanged into the zeolite according to

$$lH^+(S) + mHis^+(S) + nCu(His)_2^+(S) + (l+m+n)Na^+(Z) \leftrightarrow (l+m+n)Na^+(S) + nCu(His)_2^+(Z) + mHis^+(Z) + lH^+(Z) \quad (3)$$

and then it loses one ligand in the intra-zeolite reaction:

$$kCu(His)_2^+(Z) + kH^+(Z) \leftrightarrow kCu(His)^+(Z) + kHis^+(Z) \quad (4)$$

In this model the bis-complex transforms into the mono-complex in the zeolite. This model implies that at low Cu(II) concentrations, $l \sim n \sim k$ and reaction 4 goes forward. In contrast, at higher Cu(II) concentrations $l \ll n$, the H^+ concentration in the zeolite is low, and reaction 4 does not take place. Hence, at low Cu(II) concentration we expect the amount of Na(I) ions coming out of the zeolite after the exchange to be larger than the total amount of His in the zeolite. This is indeed experimentally observed.

Alternatively, in the second model the complex that is exchanged into the zeolite is the mono-complex (complex **A**) rather than the bis-complex due to its significantly smaller size. Although the exchange solution contains considerably larger amounts of the bis-complex, the minute amounts of the mono-complex will be preferentially exchanged due to the high selectivity of the zeolite for the smaller mono-complex according to

$$lH^+(S) + mHis^+(S) + nCu(His)^+(S) + (l+m+n)Na^+(Z) \leftrightarrow (l+m+n)Na^+(S) + nCu(His)^+(Z) + mHis^+(Z) + lH^+(Z) \quad (5)$$

Then the following intrazeolite reaction can take place:

$$kCu(His)^+(Z) + kHis^+(Z) \leftrightarrow kCu(His)_2^+(Z) + kH^+(Z) \quad (6)$$

According to this model, reaction 6 will occur when the zeolite contains low levels of H^+. This model implies that at higher Cu(II) concentration in the exchange solution the amount of Cu(II) exchanged exceeds significantly that of H^+, namely $l < n$. Although our results do not allow us to unambiguously determine which model is in effect, we prefer the first since the exchange solution contains considerably more bis-complex than mono-complex. This should compensate for the steric hindrance that is expected to slow the exchange rate of the bis-complex relative to the mono-complex. We thus conclude that the formation of complexes **A** and **B** is dictated by the delicate balance between the amounts of co-exchanged positively charged CuHis complex, H^+ and His^+. The latter is determined by the solution pH combined with pore size of the zeolite and the Cu(II) exchange level.

Conclusions

Preformed positively charged CuHis complexes were exchanged into NaY zeolite at pH 7.3. Two different complexes, their structures clearly differing from the prevailing structure in the solution, were found in the zeolite supercage. One is a mono-His complex where both the amino and imino nitrogens of the His are coordinated and the other equatorial ligands are provided by a zeolite oxygen and a water molecule. The second complex is a bis-His situated in the center of the supercage where all equatorial coordination sites are provided by the His molecules, the amino and imino nitrogens of one His molecule, and the imino nitrogen and carboxylate oxygen of the second His molecule. The mono-complex is stabilized by the presence

(36) Pöple, A.; Hartman, M.; Böhlman, W.; Böttcher, R. *J. Phys. Chem.* **1998**, *102*, 3599−3606.
(37) Pöple, A.; Gutjahr, M.; Hartman, M.; Böhlman, W.; Böttcher, R. *J. Phys. Chem.* **1998**, *102*, 7752−7763.

of protons in the zeolite which are co-exchanged with positively charged CuHis complexes and free His^+ into the zeolite. Accordingly, variations in the Cu(II) concentration and pH of the exchange solution lead to changes in the relative amounts of the two CuHis complexes in zeolite.

Acknowledgment. This work was partially supported by the MINERVA foundation. We are grateful to Dr. I. Gromov for his help with the ENDOR measurements. B.M.W. acknowledges the Fonds voor Wetenschappelijk Onderzoek (F.W.O.) for a position as postdoctoral research fellow. This work was sponsored by the Belgian Government in the frame of an Interuniversitary Attraction Pole (I.U.A.P.).

JA002572P